APL Energy

RESEARCH ARTICLE | AUGUST 18 2025

Drift-diffusion modeling of perovskite solar cells: A systematic approach

Special Collection: Novel Simulation Approaches of Perovskite Optoelectronic Devices and Materials

S. Heester ; F. Ventosinos; L. Gil-Escrig; M. Sessolo ; H. J. Bolink ; L. J. A. Koster

APL Energy 3, 036106 (2025)
https://doi.org/10.1063/5.0268013

Drift-diffusion modeling of perovskite solar cells: A systematic approach

Cite as: APL Energy 3, 036106 (2025); doi: 10.1063/5.0268013
Submitted: 27 February 2025 • Accepted: 21 July 2025 •
Published Online: 18 August 2025

S. Heester,[1] F. Ventosinos,[2] L. Gil-Escrig,[2] M. Sessolo,[2] H. J. Bolink,[2] and L. J. A. Koster[1,a)]

AFFILIATIONS

[1] Zernike Institute for Advanced Materials, University of Groningen, Nijenborgh 3, 9747AG Groningen, The Netherlands
[2] Instituto de Ciencia Molecular, Universidad de Valencia, C/Catedrático J.Beltrán 2, 46980 Paterna, Spain

Note: This paper is part of the Special Topic on Novel Simulation Approaches of Perovskite Optoelectronic Devices and Materials.
[a)]**Author to whom correspondence should be addressed:** l.j.a.koster@rug.nl

ABSTRACT

Perovskites are one of the most promising materials for the next generation of solar cells. They have high absorption coefficients, tunable bandgaps, and are versatile. However, there are still challenges regarding performance and resolving issues such as stability and degradation. To solve these challenges, a deep understanding of the inner workings of these devices is essential. Using numerical drift-diffusion simulations in combination with experimental data is an excellent approach to tackle this. However, doing this in an effective and careful way requires a rigid and thorough approach. Here, we define and demonstrate a systematic and elaborate approach for drift-diffusion modeling of perovskite solar cells (PSCs), taking into account the accuracy and repeatability of the experimental data. The approach goes beyond obtaining just a good fit with a single set of parameters but rather a unique scenario that addresses the reliability and interpretability of the obtained results. We demonstrate the effectiveness of a systematic approach by applying it to a state-of-the-art PSC, where, upon adding various amounts of chloride during the perovskite evaporation, a large change in open-circuit voltage was observed. We show that using drift-diffusion simulations, this can be explained by an increased energy step between the conduction bands of the perovskite and the electron transport layer upon increased chloride addition. When following this systematic approach, drift-diffusion modeling becomes a very powerful tool to push the limits of efficiency for PSCs.

Perovskite solar cells (PSCs) offer outstanding optoelectronic properties and high power conversion efficiency (PCE) comparable to traditional silicon-based cells, with potential for further improvement.[1–8] Perovskite materials stand out because of their excellent light absorption properties across a broad spectrum and their suitability for various promising applications, such as tandem solar cells.[9] Their low-cost fabrication methods also make them economically attractive for renewable energy systems.[10,11] However, there are still many challenges in achieving high PCEs and in solving issues such as stability, durability, and material toxicity.[12–15]

Addressing these challenges and resolving the issues has been a key topic of interest in the field of PSCs, especially in light of recombination processes, interface engineering, and the role of mobile ions and other non-idealities.[16–21] While experiments provide valuable insight into device behavior, they inherently include experimental uncertainties, which complicate the interpretation of observed trends. In addition to this, these experimental results often contain deeper layers of valuable information, especially when combined; however, they are often not immediately apparent from the data and difficult to extract.

To really improve device performance, we need a deep understanding of the inner workings and origin of losses in a device. This is often difficult due to the complexity and many correlated processes in these devices. Numerical modeling in the form of drift-diffusion simulations is a widespread and proven method to achieve this. It has been shown to, in combination with experimental measurements and observations, provide detailed insights into device behavior, loss mechanisms, and the interplay of electronic and ionic effects.[22–29]

The drift-diffusion model describes the transport, recombination, and collection of charge carriers within a device. The model is based upon the coupled Poisson and continuity equations in combination with suitable boundary conditions. What makes the

drift-diffusion model in particular a very useful and valuable tool is that its parameters carry explicit and clear physical meaning, such as carrier mobilities, trap states in both the bulk perovskite and the interfaces between layers, doping concentrations, and more. This enables the establishment of relations between micro-scale processes and the macroscopic behavior of a cell.

However, the power of fitting experimental data with the drift-diffusion model strongly depends on the robustness of the fitting and optimization procedure. In particular, typical approaches that fit specific current–voltage (JV) curves often report only one "best-fit" parameter set without fully addressing the impact of experimental uncertainty and accuracy, which can lead to ambiguous or even misleading interpretations of the underlying physics. Or the effect and impact of defining the parameter space are underestimated, while if not done properly, it can easily lead to tunnel vision or ambiguous conclusions and observations. Even the now very popular optimization strategy of Bayesian optimization (BO), while undoubtedly being highly useful and efficient, has these same pitfalls as any other fitting algorithm.

Here, we introduce a systematic approach to quantify how much reliable, physically meaningful information can actually be extracted from experimental data, taking into account the spread in experimental data.[30] Such an approach is crucial for establishing whether there exists a unique and physically consistent scenario that can explain the observed behavior, rather than merely producing a set of numbers that fit the data. By going beyond just descriptive fits, this methodology enables deeper insight into the physical processes in perovskite solar cells and shows that the fitting algorithm itself is of secondary importance.

The systematic approach follows a structured sequence of three major steps:

1. Preamble:
   (a) First, a clear definition is needed of which parameters in the model are fixed, those that can reasonably be assumed to be known, and which are free. In addition to this, the allowed ranges for the free parameters must also be specified. These choices are guided by physical considerations as well as existing literature or prior experimental knowledge. This step, where the parameter space is delineated, is fundamental and applies to any optimization procedure.
   (b) Next, a metric for the fitting error or quality of the fit must be defined, together with defining what constitutes an acceptable fit. This involves assessing the accuracy and repeatability of the experimental data to determine the expected experimental spread. A fit is considered acceptable only if it falls within this margin of variability. The purpose here is not to extract a single "best fit" solution but to understand the range of parameter sets that are consistent with the experimental data given its uncertainty.

2. The second step in the approach is to do the fitting to the experimental data. Here, one can use a relevant and suitable fitting algorithm or process of choice, such as an exploration–exploitation method based on simulated annealing[31] or BO, as the exact method is of lesser importance given the same underlying (drift-diffusion) model.

3. In the last step, analysis of the collection of accepted fits is needed to determine whether a unique physical scenario can be identified, given the accuracy of the experimental data as defined in step 1. The goal is not to obtain a single set of parameters but to establish whether a consistent interpretation of the data can be made, given the constraints and uncertainties. The main question we try to answer with this approach is how much information can be extracted from the experimental data, given its inherent error and variability? This is a crucial consideration that goes beyond simply obtaining good fits, as it addresses the reliability and interpretability of the obtained results.

For the drift-diffusion simulations, we use the one-dimensional drift-diffusion simulation software SIMsalabim.[32] There are several packages and implementations of the drift-diffusion model that could have been used, such as Setfos,[33] IonMonger,[34] Driftfusion,[35] or SCAPS;[36] however, we chose SIMsalabim as it combines several strong advantages. First, SIMsalabim is completely open-source and transparent, which facilitates usability, reproducibility, and verifiability. Second, SIMsalabim incorporates many relevant physical processes, such as mobile ionic species and an advanced description of interfacial recombination, enabling accurate modeling of device behavior and physics. Third, the software is scriptable, which is essential for automated fitting procedures and methods. Finally, SIMsalabim is compiled, resulting in fast execution times that enable efficient handling of large numbers of simulations required for global fitting.

To demonstrate the approach, we apply it to a use case with state-of-the-art PSCs where we studied the effect of chloride (Cl) addition on the performance of the cells by fitting JV curves with drift-diffusion simulations. The PSCs were prepared via co-evaporation in a *pin* structure, where *i* represents the perovskite layer and *p* and *n* represent the hole transport layer (HTL) and electron transport layer (ETL), respectively. The perovskite is $FA_{0.8}Cs_{0.2}Pb(I:Br:Cl)_3$ and was deposited by co-evaporation of CsI, formamidinium iodide, and a mixture of PbI_2, $PbBr_2$, and $PbCl_2$ using a protocol adapted from previous reports.[37,38] The thickness of the perovskite layer is 500 nm. The HTL consists of a 10 nm $N4,N4,N4'',N4''$-tetra([1,1′-biphenyl]-4-yl)-[1,1′:4′,1″-terphenyl]-4,4″-diamine (TaTm) layer, and the ETL of a 20 nm C_{60} layer. As contacts, indium tin oxide (ITO) combined with a thin layer of 2,2′,2″-(cyclopropane-1,2,3-triylidene)tris (2-(pcyanotetrafluorophenyl)acetonitrile) (CS90112) was used as the anode, and silver (Ag) combined with a thin layer of bathocuroine (BCP) as the cathode. A schematic illustration of the perovskite cell structure is depicted in Fig. S1.

To study the effect of Cl on cell performance, three different amounts were added to the lead halide mixture. The Cl content for each sample can be found in Table S1, which shows the weight relations of the individual components within the lead halide mixture. The bandgap for each sample changes only slightly upon Cl addition, as shown in Fig. 1, where we also observe a small redshift for the sample with 0.2 Cl and a small blue shift for the 0.6 Cl sample.

Upon increasing the Cl content, we observed an initial rise followed by a significant drop in open-circuit voltage (V_{oc}), as shown in Fig. 1. We will use the systematic approach with drift-diffusion

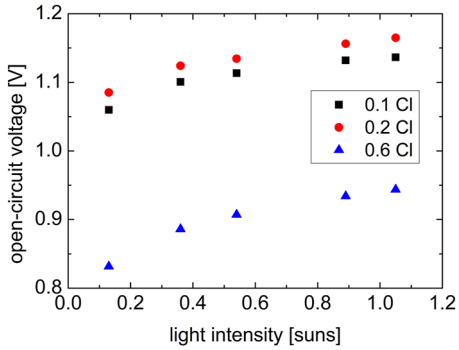

FIG. 1. V_{oc} for three samples with different amounts of Cl during evaporation (0.1, 0.2, and 0.6 Cl in weight relation as specified in Table S1) for different light intensities. When using the highest amount of Cl, we observe a significant drop in V_{oc} of ~0.2 V for all light intensities.

modeling to explain the reason and process behind this variation in V_{oc}.

The first step is defining the parameter space, a step that must not be taken lightly and can alter or bias the rest of the approach significantly. As the drift-diffusion model depends on over 50 physical parameters, the available free parameter space needs to be narrowed down. Varying and fitting all of these parameters would render it computationally impossible to perform and also unnecessarily complicated, as not every parameter holds equal relevance or importance. Hence, a decision per parameter must be made on whether it needs to be included as a free parameter or not. In the latter case, the parameter value is set as a fixed value and must be either measured or approximated. Deciding whether a parameter is free or not requires careful consideration, as this choice can greatly alter or steer the outcome and is usually based on either device knowledge or on the literature. The selected free parameters in this work are listed in Table I, and the remainder of the relevant parameters are found in Table S2.

In addition to the choice of free parameters, the respective bounds must be decided. This choice must also be a balance between accuracy, computational load, and relevance. Similar to the choice of free parameters, choices made here can greatly steer or alter the direction and outcome of the simulations. Choosing the bounds too narrowly will greatly bias the fitting direction, while taking the bounds too large will decrease the accuracy of the selected parameter, or an exponential growth of the number of simulations to be run in the next step is needed to keep the same parameter spacing and accuracy. The bounds for the chosen free parameters are also shown in Table I.

With the parameter space defined, we need to set the criteria on characterization of the performance of the cell and the quality of a simulated JV curve. To assess the quality of a complete simulated JV curve, instead of just using V_{oc}, the short-circuit current density (J_{sc}), and the fill factor (FF), we introduce a quantitative measure called the fit-error ε, defined as the normalized area between the experimental and simulated JV curve, as illustrated in Fig. 2. This metric offers equal consideration to deviations in current density as well as variations in applied voltage. The corresponding expression for the fit-error is

$$\varepsilon = \frac{\int |J_{\mathrm{sim}} - J_{\mathrm{exp}}| \mathrm{d}V}{(J_{\mathrm{max}} - J_{\mathrm{min}})(V_{\mathrm{min}} - V_{\mathrm{max}})}, \tag{1}$$

where J_{sim} is the current density of the simulated curve, J_{exp} is the current density of the experimental curve, and $J, V_{\mathrm{min,max}}$ are the maximum and minimum current density and voltage of either the simulated or experimental JV curve.

With the quantification of the quality of a simulated curve, there is still the need to determine when a simulated curve is good enough to be an accurate representation of the experimental curves. As humans, we are very well able to visually assess this, but for automated fitting, a quantitative measure in the form of a threshold value

TABLE I. Selected free parameters of the drift-diffusion model as implemented in SIMsalabim to be used as fit parameters in the simulations with their corresponding lower and upper bounds.

Parameters		Lower bound	Upper bound
Electron mobility perovskite	$\mu_{\mathrm{n}}^{\mathrm{pvsk}}$ (m^2/Vs)	10^{-6}	10^{-3}
Hole mobility perovskite	$\mu_{\mathrm{p}}^{\mathrm{pvsk}}$ (m^2/Vs)	10^{-6}	10^{-3}
Bulk trap density perovskite	$N_{\mathrm{t,bulk}}^{\mathrm{pvsk}}$ (m^{-3})	10^{19}	10^{23}
Trap density perovskite|HTL interface	$N_{\mathrm{t,int}}^{\mathrm{pvsk\|HTL}}$ (m^{-2})	10^{11}	10^{15}
Trap density perovskite|ETL interface	$N_{\mathrm{t,int}}^{\mathrm{pvsk\|ETL}}$ (m^{-2})	10^{11}	10^{15}
Direct recombination rate	k_{direct} ($\mathrm{m}^{-3}/\mathrm{s}$)	10^{-18}	10^{-15}
Shunt resistance	R_{shunt} (Ω/m^{-2})	10^{-2}	10^{3}
Charge mobility HTL	μ^{HTL} (m^2/Vs)	10^{-8}	10^{-6}
Charge mobility ETL	μ^{ETL} (m^2/Vs)	10^{-8}	10^{-6}
Valence band level HTL	$E_{\mathrm{v}}^{\mathrm{HTL}}$ (eV)	5.4	5.6
Conduction band level ETL	$E_{\mathrm{c}}^{\mathrm{ETL}}$ (eV)	3.9	4.3
Cation density perovskite	N_{cation} (m^{-3})	10^{20}	10^{23}
Anion density perovskite	N_{anion} (m^{-3})	10^{20}	10^{23}

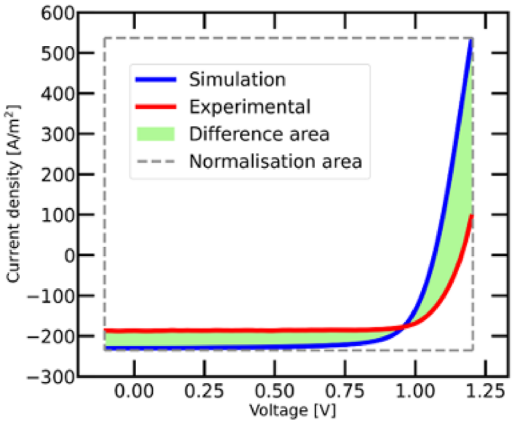

FIG. 2. Illustration of the definition of the fit-error. The fit-error is calculated by dividing the difference area between the simulated and experimental curves by the normalization area.

must be set. This value can differ per situation, including experiments or scenarios, and the choice can alter and influence drawing conclusions from the outcome. As a basis for defining this threshold, we use the observed spread in JV characteristics when repeatedly measuring the same cell, which results in a spread close to 2%, as shown in Fig. S3 for one of the samples. To account for potential other small variations, we use 2% as the absolute upper bound on the maximum allowed fit-error. To illustrate what a 2% fit-error means, we show a collection of simulated curves with varying fit errors and highlight several cases ranging from ~50% to 2% in Fig. 3. Figure 3(a) highlights a simulated curve that resulted in a large fit-error, around 50%, thus far off the experimental curve and considered a very bad fit. After slowly decreasing the fit-error by changing the parameter set, Fig. 3(f) shows the bounds that represent a 2% fit error, within which the simulated curve must lie to be considered a good fit.

To increase the reliability of the outcome of the simulations, one should fit multiple curves, experiments, or samples simultaneously, known as global fitting. This will increase the probability of finding a unique outcome or combination of parameters within the given constraints. In this work, we simultaneously fit the JV curves under five light intensities.

The second step of the approach concerns the fitting of the data. The method or algorithm is often considered to be the most important in fitting numerical simulations to experimental data; however, this is only a small part of the procedure. As mentioned before, there exist many types of algorithms and methods that are suitable and specially developed for this, each having its own benefits and downsides. However, in terms of impact on outcome and usefulness, they do not differ that much from one another, and the choice of method has a relatively limited effect on the outcome of the whole analysis, which relies much more on input and interpretation of the output.

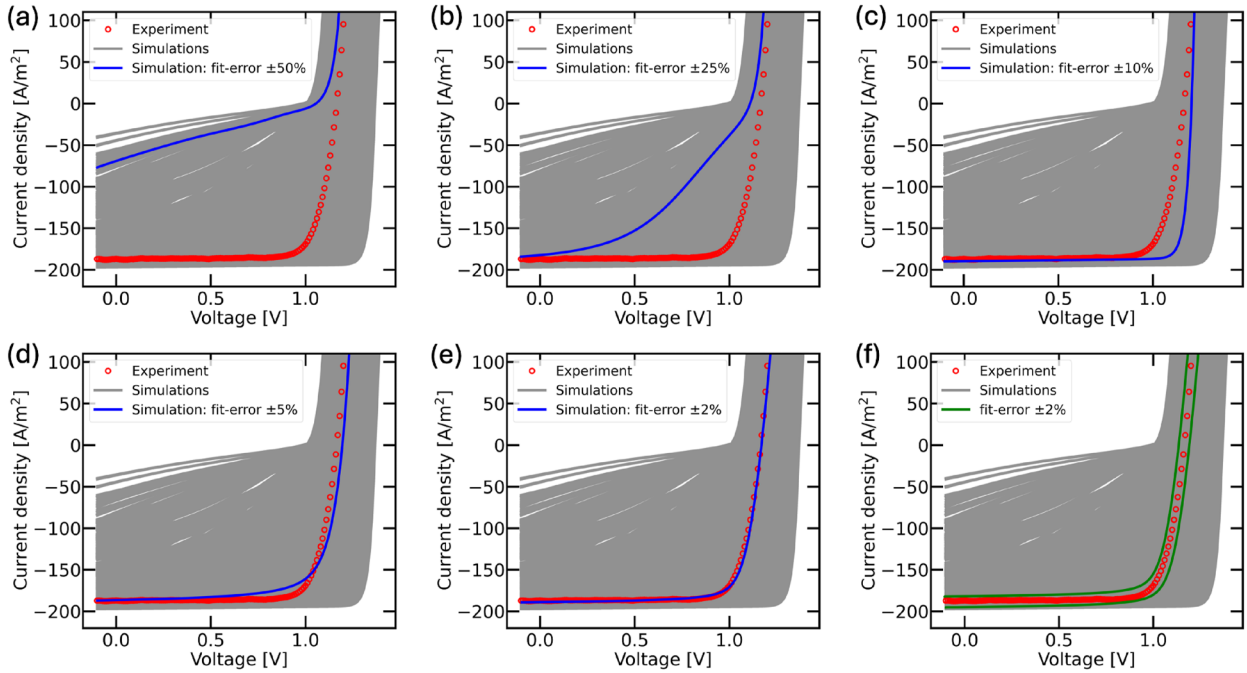

FIG. 3. JV curves to visualize the interpretation of the size of the fit-error. An experimentally measured JV curve is shown in combination with ~25 000 simulated JV curves. In panels (a)–(e), one simulated JV curve is highlighted, which represents a certain fit-error ranging from 50% to 2%. Figure (f) shows the approximate bounds within which a simulated JV curve must lie to be considered a good fit.

In this work, we employed a systematic scan over the full parameter range in combination with a more selective automated routine based on simulated annealing. The systematic scan consists of dividing the parameter space into equal segments and performing all simulations. This enables a comprehensive and unbiased exploration of the entire parameter space. However, as the number of parameters grows, the multitude of parameter combinations escalates rapidly, demanding substantial computing resources and becoming a time consuming process. Hence, we also utilized a selective automated fitting procedure. Here, we take random combinations of parameters within our parameter space and record the respective fit-error for this combination. Once the error reaches a predetermined threshold, we transition to a parameter selection method where parameters are adjusted individually, each within a few percentage points of those yielding the lowest error. This method allows us to identify parameter combinations with minimal fit-errors without scanning the entire parameter range. To mitigate the risk of encountering a local minimum in the fit-error, the automated fitting routine was run multiple times. In addition to this, we have used BO as a fitting algorithm as well, as implemented in optimPV.[39] As the underlying drift-diffusion model is the same for each method, the choice of algorithm is of lesser importance. While BO is highly efficient and quick, it also does not inherently address the central question of how much information can readily be extracted from the experiment, even being slightly less rigorous or unbiased in providing output, taking into account the entire parameter space. Nonetheless, each of the methods ultimately returned the same set of fitted parameters corresponding to the simulated JV curve with the lowest fit-error.

Moving on to the last step of the approach, we need to look at the outcome of the fitting first. The best matching simulated JV curves, thus with the lowest fit-error, are depicted in Fig. 4 together with the experimental JV curves, as obtained with the simulated annealing method. The best matching JV curves obtained with BO can be found in Fig. S4.

Each fit shows very good agreement between the simulated and experimentally measured JV curve, with a fit-error around 1%, well within our set threshold of 2%. The fitted model parameters for these curves are shown in Table S2. The rest of the model parameters, thus those that were not fitted for the samples, are shown in Table S3.

From this set of fitted parameters, one would be able to directly draw conclusions and potentially provide an explanation for the drop in V_{oc} with the increased amount of added Cl. However, we need to take into account the experimental spread and uncertainty and examine whether we can still find a unique scenario that describes the data, as outlined in step three of the approach.

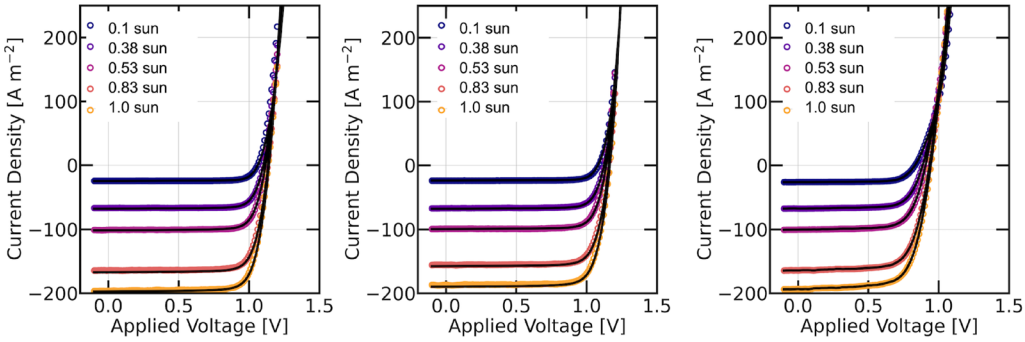

FIG. 4. Simulated JV curves with the lowest fit-error for all three samples: (a) 0.1 Cl, (b) 0.2 Cl, and (c) 0.6 Cl. The solid black lines represent the simulated JV curves, and the colored symbols represent the experimental data. Each sample shows the excellent agreement between the experimental and simulated JV curves.

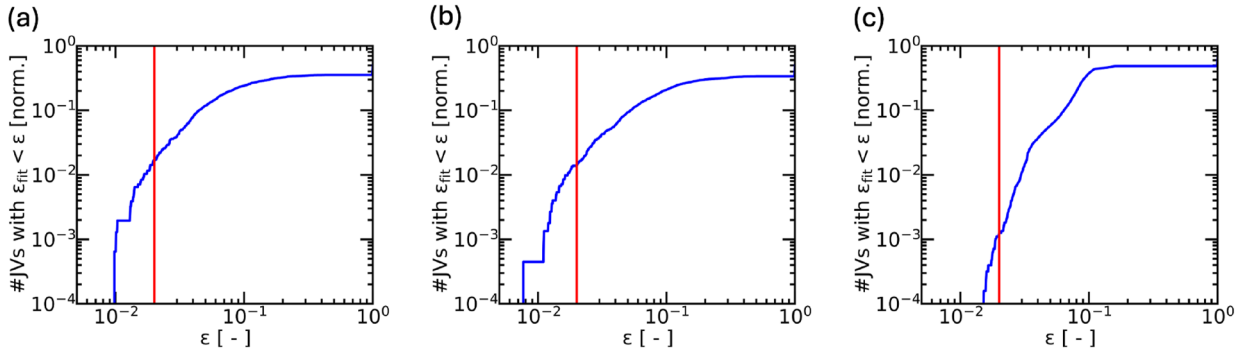

FIG. 5. Fraction of JV curves with a fit-error lower than the specified fit-error on the horizontal axis for each sample: (a) 0.1Cl, (b) 0.2Cl, and (c) 0.6Cl. The total number of simulations is ~25 000 per sample. The red line indicates the 2% fit-error. We observe that for each sample, between 0.01% and 0.1% of the total number of performed simulations had a fit-error below our defined fit-error threshold of 2%.

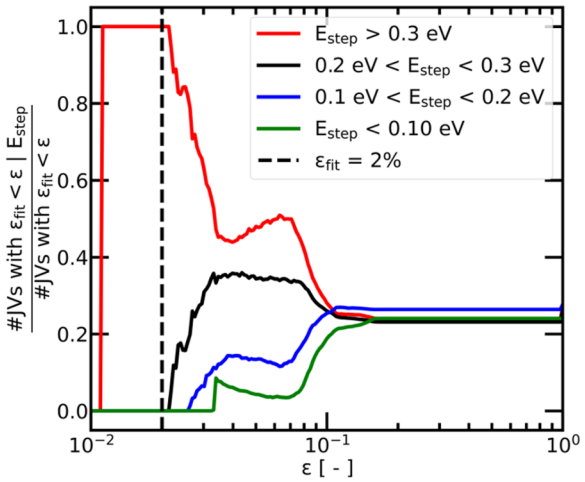

FIG. 6. Normalized number of simulated JV curves with a fit-error below a certain value indicated on the horizontal axis. Each curve represents a subset of simulated JV curves grouped by the value of the energy step between the conduction bands of the perovskite and ETL, as determined by the input of the corresponding free parameter, where each subgroup covers an interval of 0.1 eV. We see that all curves that matched the fit-error criterion of 2% had an energy step of 0.3 eV.

To achieve this, we need to first collect all curves or sets of parameters that meet our criteria. Figure 5 shows, as a function of the fit-error, the fraction of simulated JV curves that had an error below a certain fit-error.

Taking the set fit-error threshold of 2%, indicated by the vertical line, we see that we do not have just a single set of parameters that matched our criteria, but many. Depending on the defined fit-error threshold, the number of JV curves that match either decreases or increases, which can change the conclusions, as we will discuss in the next section.

The question remains whether there is then a unique scenario that provides an explanation for the drop in V_{oc}, taking into account the experimental uncertainty and accuracy. For this set of samples, a single scenario was found, namely, an increased step in energy between the conduction bands of the perovskite and the ETL, which is illustrated in Fig. 6.

In Fig. 6, we show again the fraction of JV curves with a fit-error lower than the specified fit-error on the horizontal axis, but we have now split them into four sets, grouped by the value of the energy step between the conduction bands of the perovskite and ETL, as determined by the input of the corresponding free parameter. Each subgroup covers an interval of 0.1 eV. We have then normalized the selected number of JV curves having that specific energy step to the total number of JV curves with a fit-error lower than the specified fit-error. If we then look at the section of the graph with $\varepsilon < 2\%$, we see that all of the curves had an energy step of at least 0.3 eV, which is significantly more than the energy steps between these layers for the other samples, which were between 0.05 and 0.1 eV. When we decrease the energy step, the fit-error also starts to increase, meaning they match less well with the experimental data; hence, it is important where the threshold is set. Thus, based on our choice of parameters and limits, assessment criteria, and experimental uncertainty, we can explain the observed behavior of the drop in V_{oc} with an increased energy step between the conduction bands of the perovskite and ETL.

In order to support the conclusion that the drop in V_{oc} is actually the result of the increased energy step, we simulated the cell with increased chloride content once again, but with an optimized conduction band level of the ETL of 3.92 eV. Which, taking into account the conduction band level of the perovskite of 3.96 eV, translates to an energy step of 0.04 eV above the perovskite conduction band, in relatively good accordance with findings before.[40] The results are shown in Fig. S5, where we observe that V_{oc} is greatly increased. Since the band alignment has been fully optimized, it is even higher compared to the previously best sample with 0.2 chloride content.

To place the explanation into context, chloride, when used in the fabrication process of PSCs, is typically not found in the transport layers unless it is added as a dopant.[41–43] By doping, Cl atoms induce passivation effects on defects at the perovskite-transport layer interface, thereby enhancing performance. Migration of Cl from the perovskite to the transport layers is also not a common observation. Instead, it stays in the perovskite and mainly influences the crystallization and properties of the perovskite absorber layer. However, we observed very little to no presence of Cl content in the perovskite film itself, as can be concluded from the bandgap remaining nearly constant among all three samples, despite the substantially increasing amount of chloride used during fabrication, as shown in Fig. S2. This implies that the chloride is not in the final perovskite and either migrated toward one or both of the transport layers or is no longer present in the device but still affected the properties of the cell, though.

Chloride migration toward the transport layers has been observed in perovskite cells where TiO_2 was used as ETL and 2,2′,7,7′-tetrakis-(N,N-di-4-methoxyphenylamino)-9,9′-spirobifluorene (Spiro-OMeTAD) as HTL, where it tends to favorably interact with the ETL, leading to better alignment between the energy bands of the transport layers and the perovskite.[44,45] This indicates a movement of the conduction band level of the ETL toward that of the perovskite. In addition to this, a deepening of the Fermi level of the HTL has been observed, resulting in an enlargement of the built-in potential, thereby further enhancing performance. An important distinction with our samples lies in the use of organic transport layers, as opposed to the inorganic transport layers such as TiO_2 utilized in these situations. Since the organic and inorganic transport layers can have quite different behavior, this might be a lead toward the observed negative effect on the performance of the device instead of the expected positive effect.

In this work, we have described a systematic approach to use drift-diffusion modeling to obtain a deep understanding of perovskite solar cells and gain insight into their behavior and limitations. The method helps to answer the question of how much information one can retrieve from fitting experimental data given the experimental uncertainty and repeatability. We show that the choice of fitting algorithm, whether simulated annealing, BO, or something else, is of secondary importance. We have shown that defining the parameter space, setting assessment criteria, and the interpretation of the outcome are essential parts of the fitting

process, and they steer and influence the quality and effectiveness of the outcome. We have demonstrated the approach using a state-of-the-art co-evaporated perovskite solar cell, where a varying amount of added chloride during evaporation resulted in significant changes in V_{oc}. We were able to provide an explanation for this in the form of an increased energy step between the conduction bands of the perovskite and ETL and have shown that even though many sets of fitted parameters matched our criteria, this was a unique solution taking into account our defined parameters, assessment criteria, and experimental uncertainty.

The supplementary material includes the full cell architecture and more detailed material compositions in terms of the lead halide mixture and is complemented with several additional experimental measurements of the cell. Furthermore, the complete sets of SIMsalabim model parameters for each cell are given.

This work is funded by the European Union; views and opinions expressed are, however, those of the authors only and do not necessarily reflect those of the European Union or CINEA; neither the European Union nor the granting authority can be held responsible for them. The NEXUS project has received the funding from the Horizon Europe Research and Innovation Action program under Grant Agreement No. 101075330. The authors thank the Center for Information Technology of the University of Groningen for their support and for providing access to the Hábrók high performance computing cluster. M.S. acknowledges the funding from the Comunitat Valenciana (Grant No. CISEJI/2022/43).

AUTHOR DECLARATIONS

Conflict of Interest

The authors have no conflicts to disclose.

Author Contributions

S. Heester: Conceptualization (lead); Formal analysis (equal); Funding acquisition (equal); Software (equal); Supervision (lead); Writing – original draft (lead); Writing – review & editing (equal). **F. Ventosinos**: Formal analysis (equal); Investigation (equal); Software (equal); Writing – original draft (lead); Writing – review & editing (supporting). **L. Gil-Escrig**: Investigation (supporting); Writing – review & editing (supporting). **M. Sessolo**: Investigation (supporting); Supervision (supporting); Writing – review & editing (supporting). **H. J. Bolink**: Funding acquisition (lead); Supervision (equal); Writing – review & editing (equal). **L. J. A. Koster**: Conceptualization (lead); Formal analysis (equal); Funding acquisition (equal); Software (equal); Supervision (lead); Writing – review & editing (supporting).

DATA AVAILABILITY

The data that support the findings of this study are available within the article and will be openly available at the University of Groningen's repository DataverseNL.

REFERENCES

[1] Y. Rong, Y. Hu, A. Mei, H. Tan, M. I. Saidaminov, S. I. Seok, M. D. McGehee, E. H. Sargent, and H. Han, "Challenges for commercializing perovskite solar cells," Science **361**, eaat8235 (2018).
[2] K. Artuk, D. Turkay, M. D. Mensi, J. A. Steele, D. A. Jacobs, M. Othman, X. Yu Chin, S.-J. Moon, A. N. Tiwari, A. Hessler-Wyser *et al.*, "A universal perovskite/C_{60} interface modification via atomic layer deposited aluminum oxide for perovskite solar cells and perovskite–silicon tandems," Adv. Mater. **36**, 2311745 (2024).
[3] J. Y. Kim, J.-W. Lee, H. S. Jung, H. Shin, and N.-G. Park, "High-efficiency perovskite solar cells," Chem. Rev. **120**, 7867–7918 (2020).
[4] G. Wu, R. Liang, M. Ge, G. Sun, Y. Zhang, and G. Xing, "Surface passivation using 2D perovskites toward efficient and stable perovskite solar cells," Adv. Mater. **34**, 2105635 (2022).
[5] Z. Chen, B. Turedi, A. Y. Alsalloum, C. Yang, X. Zheng, I. Gereige, A. AlSaggaf, O. F. Mohammed, and O. M. Bakr, "Single-crystal $MAPbI_3$ perovskite solar cells exceeding 21% power conversion efficiency," ACS Energy Lett. **4**, 1258–1259 (2019).
[6] M. R. Filip, G. E. Eperon, H. J. Snaith, and F. Giustino, "Steric engineering of metal-halide perovskites with tunable optical band gaps," Nat. Commun. **5**, 5757 (2014).
[7] M. A. Green and A. Ho-Baillie, "Perovskite solar cells: The birth of a new era in photovoltaics," ACS Energy Lett. **2**, 822–830 (2017).
[8] M. T. Hörantner, T. Leijtens, M. E. Ziffer, G. E. Eperon, M. G. Christoforo, M. D. McGehee, and H. J. Snaith, "The potential of multijunction perovskite solar cells," ACS Energy Lett. **2**, 2506–2513 (2017).
[9] H. S. Jung and N.-G. Park, "Perovskite solar cells: From materials to devices," Small **11**, 10–25 (2015).
[10] M. Cai, Y. Wu, H. Chen, X. Yang, Y. Qiang, and L. Han, "Cost-performance analysis of perovskite solar modules," Adv. Sci. **4**, 1600269 (2017).
[11] L. A. Zafoschnig, S. Nold, and J. C. Goldschmidt, "The race for lowest costs of electricity production: Techno-economic analysis of silicon, perovskite and tandem solar cells," IEEE J. Photovoltaics **10**, 1632–1641 (2020).
[12] D. Wang, M. Wright, N. K. Elumalai, and A. Uddin, "Stability of perovskite solar cells," Sol. Energy Mater. Sol. Cells **147**, 255–275 (2016).
[13] Z. Xiao, Z. Song, and Y. Yan, "From lead halide perovskites to lead-free metal halide perovskites and perovskite derivatives," Adv. Mater. **31**, 1803792 (2019).
[14] G. Schileo and G. Grancini, "Lead or no lead? Availability, toxicity, sustainability and environmental impact of lead-free perovskite solar cells," J. Mater. Chem. C **9**, 67–76 (2021).
[15] J.-P. Correa-Baena, M. Saliba, T. Buonassisi, M. Grätzel, A. Abate, W. Tress, and A. Hagfeldt, "Promises and challenges of perovskite solar cells," Science **358**, 739–744 (2017).
[16] T. S. Sherkar, C. Momblona, L. Gil-Escrig, J. Ávila, M. Sessolo, H. J. Bolink, and L. J. A. Koster, "Recombination in perovskite solar cells: Significance of grain boundaries, interface traps, and defect ions," ACS Energy Lett. **2**, 1214–1222 (2017).
[17] J. M. Cave, N. E. Courtier, I. A. Blakborn, T. W. Jones, D. Ghosh, K. F. Anderson, L. Lin, A. A. Dijkhoff, G. J. Wilson, K. Feron *et al.*, "Deducing transport properties of mobile vacancies from perovskite solar cell characteristics," J. Appl. Phys. **128**, 184501 (2020).
[18] V. M. Le Corre, M. Stolterfoht, L. Perdigón Toro, M. Feuerstein, C. Wolff, L. Gil-Escrig, H. J. Bolink, D. Neher, and L. J. A. Koster, "Charge transport layers limiting the efficiency of perovskite solar cells: How to optimize conductivity, doping, and thickness," ACS Appl. Energy Mater. **2**, 6280–6287 (2019).
[19] J. Thiesbrummel, S. Shah, E. Gutierrez-Partida, F. Zu, F. Peña-Camargo, S. Zeiske, J. Diekmann, F. Ye, K. P. Peters, K. O. Brinkmann *et al.*, "Ion-induced field screening as a dominant factor in perovskite solar cell operational stability," Nat. Energy **9**, 664–676 (2024).
[20] J. Wu, L. Torresi, M. Hu, P. Reiser, J. Zhang, J. S. Rocha-Ortiz, L. Wang, Z. Xie, K. Zhang, B.-w. Park *et al.*, "Inverse design workflow discovers hole-transport materials tailored for perovskite solar cells," Science **386**, 1256–1264 (2024).
[21] O. Malinkiewicz, A. Yella, Y. H. Lee, G. M. Espallargas, M. Graetzel, M. K. Nazeeruddin, and H. J. Bolink, "Perovskite solar cells employing organic charge-transport layers," Nat. Photonics **8**, 128–132 (2014).

[22]C. M. Wolff, P. Caprioglio, M. Stolterfoht, and D. Neher, "Nonradiative recombination in perovskite solar cells: The role of interfaces," Adv. Mater. **31**, 1902762 (2019).
[23]D. Bartesaghi, I. del Carmen Pérez, J. Kniepert, S. Roland, M. Turbiez, D. Neher, and L. J. A. Koster, "Competition between recombination and extraction of free charges determines the fill factor of organic solar cells," Nat. Commun. **6**, 7083 (2015).
[24]S. G. McCallum, O. Nicholls, K. O. Jensen, M. V. Cowley, J. E. Lerpinière, and A. B. Walker, "Bayesian parameter estimation for characterising mobile ion vacancies in perovskite solar cells," J. Phys.: Energy **6**, 015005 (2023).
[25]W. Clarke, G. Richardson, and P. Cameron, "Understanding the full zoo of perovskite solar cell impedance spectra with the standard drift-diffusion model," Adv. Energy Mater. **14**, 2400955 (2024).
[26]T. Golubev, D. Liu, R. Lunt, and P. Duxbury, "Understanding the impact of C_{60} at the interface of perovskite solar cells via drift-diffusion modeling," AIP Adv. **9**, 035026 (2019).
[27]T. S. Sherkar, C. Momblona, L. Gil-Escrig, H. J. Bolink, and L. J. A. Koster, "Improving perovskite solar cells: Insights from a validated device model," Adv. Energy Mater. **7**, 1602432 (2017).
[28]L. Lüer, I. M. Peters, V. M. L. Corre, K. Forberich, D. M. Guldi, and C. J. Brabec, "Bypassing the single junction limit with advanced photovoltaic architectures," Adv. Mater. **36**, 2308578 (2024).
[29]M. T. Neukom, A. Schiller, S. Züfle, E. Knapp, J. Ávila, D. Pérez-del-Rey, C. Dreessen, K. P. S. Zanoni, M. Sessolo, H. J. Bolink, and B. Ruhstaller, "Consistent device simulation model describing perovskite solar cells in steady-state, transient, and frequency domain," ACS Appl. Mater. Interfaces **11**, 23320–23328 (2019).
[30]R. C. Kurchin, J. R. Poindexter, V. Vähänissi, H. Savin, C. del Cañizo, and T. Buonassisi, "How much physics is in a current–voltage curve? Inferring defect properties from photovoltaic device measurements," IEEE J. Photovoltaics **10**, 1532–1537 (2020).
[31]W. H. Press, *Numerical Recipes 3rd Edition: The Art of Scientific Computing* (Cambridge University Press, 2007).
[32]M. Koopmans, V. Corre, and L. Koster, "SIMsalabim: An open-source drift-diffusion simulator for semiconductor devices," J. Open Source Softw. **7**, 3727 (2022).
[33]Fluxim, *Setfos*, 2024.
[34]W. Clarke, L. J. Bennett, Y. Grudeva, J. M. Foster, G. Richardson, and N. E. Courtier, "IonMonger 2.0: Software for free, fast and versatile simulation of current, voltage and impedance response of planar perovskite solar cells," J. Comput. Electron. **22**, 364–382 (2023).
[35]P. Calado, I. Gelmetti, B. Hilton, M. Azzouzi, J. Nelson, and P. R. F. Barnes, "Driftfusion: An open source code for simulating ordered semiconductor devices with mixed ionic-electronic conducting materials in one dimension," J. Comput. Electron. **21**, 960–991 (2022).
[36]M. Burgelman, P. Nollet, and S. Degrave, "Modelling polycrystalline semiconductor solar cells," Thin Solid Films **361–362**, 527–532 (2000).
[37]L. Gil-Escrig, C. Dreessen, F. Palazon, Z. Hawash, E. Moons, S. Albrecht, M. Sessolo, and H. J. Bolink, "Efficient wide-bandgap mixed-cation and mixed-halide perovskite solar cells by vacuum deposition," ACS Energy Lett. **6**, 827–836 (2021).
[38]L. Gil-Escrig, I. Susic, İ. Doğan, V. Zardetto, M. Najafi, D. Zhang, S. Veenstra, S. Sedani, B. Arikan, S. Yerci *et al.*, "Efficient and thermally stable wide bandgap perovskite solar cells by dual-source vacuum deposition," Adv. Funct. Mater. **33**, 2214357 (2023).
[39]V. M. Le Corre and L. Lüer, Optimpv, *Github repository*, 2025.
[40]M. Koopmans and L. J. A. Koster, "Voltage deficit in wide bandgap perovskite solar cells: The role of traps, band energies, and effective density of states," Sol. RRL **6**, 2200560 (2022).
[41]J.-W. Liang, Y. Firdaus, R. Azmi, H. Faber, D. Kaltsas, C. H. Kang, M. I. Nugraha, E. Yengel, T. K. Ng, S. De Wolf *et al.*, "Cl_2-doped CuSCN hole transport layer for organic and perovskite solar cells with improved stability," ACS Energy Lett. **7**, 3139–3148 (2022).
[42]C. C. Lin, T. N. Murakami, M. Chikamatsu, T. Bessho, M. Furue, and H. Segawa, "A sodium chloride modification of SnO_2 electron transport layers to enhance the performance of perovskite solar cells," ACS Omega **6**, 17880–17889 (2021).
[43]E. Edri, S. Kirmayer, M. Kulbak, G. Hodes, and D. Cahen, "Chloride inclusion and hole transport material doping to improve methyl ammonium lead bromide perovskite-based high open-circuit voltage solar cells," J. Phys. Chem. Lett. **5**, 429–433 (2014).
[44]Q. Chen, H. Zhou, Y. Fang, A. Z. Stieg, T.-B. Song, H.-H. Wang, X. Xu, Y. Liu, S. Lu, J. You *et al.*, "The optoelectronic role of chlorine in $CH_3NH_3PbI_3$(Cl)-based perovskite solar cells," Nat. Commun. **6**, 7269 (2015).
[45]S. Colella, E. Mosconi, G. Pellegrino, A. Alberti, V. L. P. Guerra, S. Masi, A. Listorti, A. Rizzo, G. G. Condorelli, F. De Angelis, and G. Gigli, "Elusive presence of chloride in mixed halide perovskite solar cells," J. Phys. Chem. Lett. **5**, 3532–3538 (2014).